# Control of the supercrystallinity, nanocrystallinity, morphology and magnetism of cobalt nanoparticle assemblies. Towards novel colloidal crystals with high magnetic anisotropy

Anh-Tu Ngo, Salvatore Costanzo, Pierre-Antoine Albouy, Vincent Russier, Isabelle Lisiecki

DOI: 10.1016/j.colsurfa.2022.128578

# Control of the Supercrystallinity, Nanocrystallinity Morphology and Magnetism of Cobalt Nanoparticle Assemblies. Towards Novel Colloidal Crystals with High Magnetic Anisotropy

Anh-Tu Ngo[1], Salvatore Costanzo[1], Pierre-Antoine Albouy[2], Vincent Russier[3]* and Isabelle Lisiecki[1]*

1-Sorbonne Université, CNRS, De la Molécule aux Nano-Objets: Réactivité, Interactions Spectroscopies, MONARIS, 75005, Paris France

2- Laboratoire de Physique des Solides, CNRS, Université Paris-Sud, Université Paris-Saclay, 91405 Orsay, France

3- ICMPE UMR 7182 CNRS and Université UPE, 2-8 rue Henri Dunant, 94320 Thiais, France.

* Address correspondence to isabelle.lisiecki@sorbonne-universite.fr and vincent.russier@cnrs.fr

## ABSTRACT

Starting from a colloidal solution of dodecanoic acid-coated Co nanoparticles (NP) of 8.1 nm in size and of low anisotropy and using a solvent-mediated ligand-ligand interaction strategy, we obtain either colloidal crystals or supercrystalline films. The comparison between the structural and magnetic properties of these two different architectures of supercrystals evidences improved magnetic properties for the colloidal crystals. This is interpreted as a result of both an increase in the mesoscopic coherence length and a decrease in the interparticle distance. In this work we extend this comparative study between the two types of supercrystals after annealing treatment. A common batch of NP is used for the native and the annealed samples in order to optimize the accuracy of the comparison. A complete set of structural characterizations and magnetic measurements shows that upon annealing the NP evolve from soft to hard magnetic NP, with changes of both the anisotropy constant and saturation mangnetization, while the supercrystal structures remain unchanged. Both native and annealed colloidal crystals remain characterized by a smaller interparticle distance compared to the corresponding films, inducing higher dipolar interactions, which is evidenced by an increase in the blocking temperature. In this study, we highlight the first fcc colloidal crystals made of hcp-Co single crystals resulting from the annealing of their native counterparts made of fcc-Co polycrystals. In addition, the comparative magnetic study between both the annealed supercrystalline films and colloidal crystals evidences enhanced magnetic properties for the latter ones.

**Keywords:** fcc-Co, hcp-Co, nanoparticles, annealing, fcc colloidal crystals, coherence length, anisotropy, dipolar interaction

## 1. Introduction

Self-assemblies of alkyl chains coated inorganic nanoparticles (NPs) into micrometer-scale ordered assemblies arrays constitute attractive advanced materials with an interplay of the intrinsic NPs properties and their collective interactions. This results in new mechanical [1], transport [2], optical, vibrational [3], chemical (stability against oxidation and coalescence) [4] and magnetic properties [5]. Depending on the deposition strategy, small isolated colloidal single crystals or a homogeneous film made of contiguous supercrystalline domains can be obtained. This difference reflects two different growth processes that can be activated by controlling the alkyl chains coated NPs solvation, i.e, ligand-ligand interactions: *1)* heterogeneous nucleation onto the substrate that results in a continuous film or *2)* homogeneous nucleation in solution that results in the deposition of isolated crystals. The first example of a film made of magnetic NPs packed into 3D-ordered domains has been published in 2003 [6]. It has been shown that these artificial solids, made of several hundred monolayers of fcc-Co NPs and ordered at a mesoscale into an fcc superstructure, have specific magnetic properties. Thereafter, magnetic supercrystal films have been also obtained using Ni [7] and maghemite [8]. Magnetic colloidal crystals have been first reported with Ni [7] NPs, followed by $Fe_3O_4$ [9] and $Fe_3O_4$-$\gamma$-$Fe_2O_3$ [10] and most of the reported study suffers of a lack of comprehensive structural study. We recently evidenced that a co-evaporation method with ethanol and hexane, allowed the growth of well-defined face-centered cubic (fcc) colloidal crystals of $\gamma$-$Fe_2O_3$ and fcc-Co NPs [11, 12]. A comparative magnetic study performed on supercrystalline films and colloidal crystals made of low anisotropy fcc-Co NPs revealed without ambiguity an enhancement of the magnetic properties in the latter case compared to the former. This resulted from an improved mesoscopic packing of NPs and a decrease in the interparticle distance. Since high magnetic anisotropy materials are highly required for some applications, in this paper our purpose is to tune the nanocristallinity of the particles from poorly

anisotropic fcc polycrystals to highly anisotropic hexagonal compact packing (hcp) single-crystals. This is done by annealing the NP at 350 °C. Both comparative structural and magnetic studies of native and annealed supercrystalline films and colloidal crystals are performed, using the same batch of particles. For the first time, we highlight that the colloidal crystals of hcp-Co single crystals exhibit optimized structural properties (higher coherence length, hcp-Co single crystals and smaller interparticle gap distance). These enhanced structural properties induces higher dipolar interactions, evidenced by a higher blocking temperature.

## 2. Experimental Section

*2.1. Chemical*

All materials were used as purchased without further purification. Cobalt acetate and ethanol (VWR), isooctane and hexane (Sigma Aldrich), sodium di(ethylhexyl) sulfosuccinate (Na(AOT)) (Fluka), and sodium borohydride dodecanoic acid (Acros). The synthesis of cobalt(II) bis(2-ethylhexyl)sulfosuccinate, ($Co(AOT)_2$) has been described previously.

*2.2. Synthesis of Dodecanoic Acid Coated 8.1 nm-Co NPs*

Cobalt NPs stabilized by dodecanoic acid chains are synthesized by chemical reduction in reverse micelles (water in oil droplets) as described in a previous paper [13]. The size polydispersity is optimized by controlling the reducing agent (sodium borohydride) concentration. The NPs are dispersed in hexane. Their mean diameter and size polydispersity are equal to 8.1 nm and 11%, respectively.

*2.3. Synthesis of 3D fcc Supercrystalline Film of 8.1 nm-Co NPs*

The 3D supercrystalline films are obtained by immersing the HOPG (Highly ordered pyrolytic graphite) substrate in 200 µl of a 8 $10^{-3}$ M colloidal nanocrystal solution (5.5 x 10-7 M particles). The

substrate temperature is fixed at 35 °C and the solvent evaporation, takes place under nitrogen and lasts around 24h [6].

*2.4. Synthesis of Colloidal Crystals made of 8.1 nm-Co NPs*

Colloidal crystals made of 8.1 nm-Co NPs are produced by ethanol-induced precipitation diffusion of ethanol vapor into a NPs colloidal solution [12]: One beaker (*beaker 1*) is filled with 200 µL of a NP (6 $10^{-3}$ M of atomic cobalt) colloidal solution in hexane, at the bottom of which a silicon wafer is positioned horizontally. Another beaker (*beaker 2*), having the same size, is filled with 100 µL of ethanol (99.8%). The two beakers 1 and 2 are positioned into a third one, which is sealed and left at room temperature. During evaporation in beaker 1, hexane progressively enriches with ethanol. Total evaporation of the solvent (mixture of ethanol and hexane**)** in beaker 1 occurs within approximately 20 h.

*2.5. Annealing of the Colloidal Crystals of 8.1 nm Co NPs*

The colloidal crystals deposited on a Si substrate are annealed in a nitrogen filled quartz ampoule for 15 min in a furnace at 350 °C [14].

*2.6. Apparatus*

A JEOL (100 kV) transmission electron microscopy model JEM-1011 is used to determine the size of Co NPs.

The 3D supercrystalline films and the colloidal crystals are visualized using a scanning electron microscope (SEM, JEOL 5510 LV) and a field emission gun scanning electron microscope (FEG-SEM, Hitachi Su-70).

Grazing Incidence Small-angle X-ray scattering (GISAXS) measurements have been described in details in Ref. [11].–

The magnetization of the 3D supercrystalline films and the colloidal crystals are measured using

a commercial vibrating sample magnetometer (VSM) from Quantum design. All magnetic measurements are carried out with the applied field parallel to the substrate. The susceptibility *versus* temperature is measured by a zero-field cooled (ZFC)/field cooled (FC) experiment. In the ZFC measurement, the sample is cooled down to 3 K without an applied field starting from 300 K (where all the particles are in the superparamagnetic state). Afterwards the magnetization $M_{ZFC}(T)$ is measured as function of the increasing temperature to 300 K in a small field of 20 Oe. Then for the FC measurement, the sample is cooled again to 3 K under the same applied field and the magnetization $M_{FC}(T)$ is recorded. Hysteresis curves with fields up to 5 T are taken at 3 K for all the samples.

## 3. Results and Discussion

### *3.1. Formation of fcc supercrystalline films and fcc colloidal crystals of 8.1 nm-$Co_{fcc}$ NPs*

#### *3.1.1. The supercrystalline films*

The supercrystalline films are prepared by a slow evaporation of a colloidal solution of fcc-Co NPs under a pure nitrogen flow [6]. The scanning electron microscopy (SEM) reveals a rather inhomogeneous film with a thickness decreasing from a few micrometers at the rim to tens of nanometers in the central part. As shown in the Figure 1a, the upper surface of the film appears heavily cracked. The corresponding grazing incidence small-angle X-ray scattering (GISAXS) pattern is characteristic of a fcc mesostructure where domains display a preferential orientation with the [111] direction perpendicular to the substrate (inset of Fig. 1a): it means that the denser (111) planes are preferentially parallel to the substrate. The Half Width at Half Maximum (HWHM) of the (111) peak is $\delta$ = 0.08 $nm^{-1}$ higher than the experimental resolution (ca. 0.05$nm^{-1}$) (Table 1) [6]. The denser plane packing periodicity is $d_{111}$=9.0 nm, that points to a centre-to-centre interparticle distance $D_{c\text{-}c}$ =11.1 nm.

The associated interparticle gap is $D_{i\text{-}p}$=3.0 nm (Table 1) and all these values are in very good agreement with data previously reported in similar supercrystalline film samples [6,14].

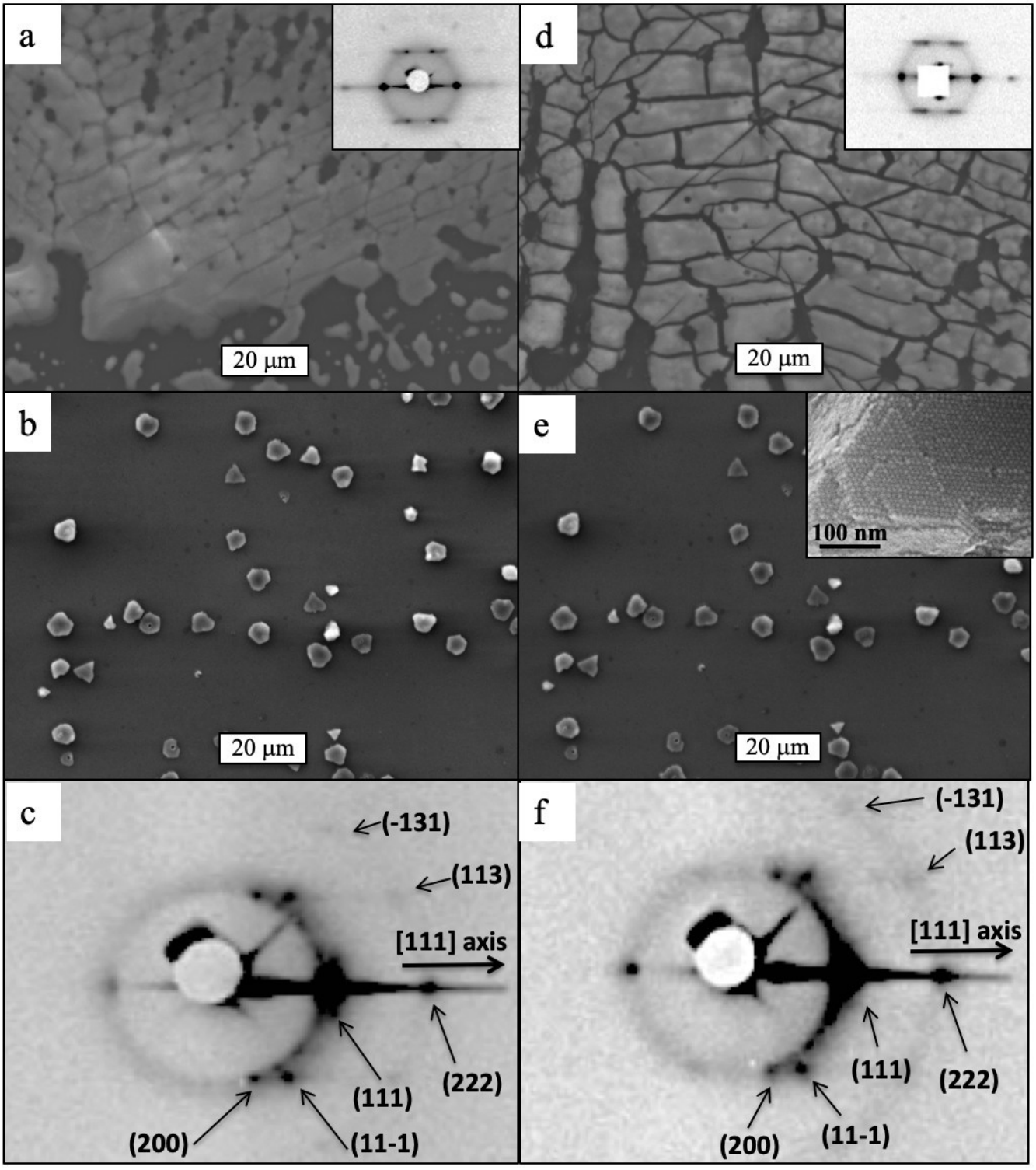


**Fig. 1.** SEM images of supercrystalline films (a) before and (d) after annealing (insets: corresponding GISAXS pattern). SEM images of colloidal crystals (b) before and (e) after annealing. Inset of Figure

1e: HR-SEM image of a regular triangle. GISAXS pattern of colloidal crystals (c) before and (f) after annealing.

*3.1.2. The colloidal crystals*

The colloidal crystals are based on Co NPs from the same batch and are obtained by ethanol-induced precipitation [12]. The NPs solution in hexane is evaporated in the presence of a second beaker containing ethanol, which progressively diffuses into the colloidal solution. After roughly 20h, the original NPs solution is liquid-free and low magnification SEM study reveals isolated NP assemblies (Fig. 1b). Various morphologies including regular triangles, truncated triangles and hexagons, are obtained. These isolated assemblies show well-developed facets, clear edges and sharp corners (Fig. 1b) and their sizes can reach up to 5 μm and display various orientations with respect to the substrate. These geometrical observations are consistent with nucleation and growth processes in solution. Similar to the film morphology, GISAXS study indicates a fcc structure (Fig. 1c). The (111) peak is now resolution-limited that indicates higher mesostructrure order compared to the supercrystalline films. In addition, the stacking periodicity in the [111] direction is now 8.7 nm that corresponds to an interparticle gap $D_{i\text{-}p}$=2.5 nm, smaller than obtained in supercrystalline films (Table 1).

The change in the sample morphology is explained by solvent-mediated ligand-ligand interaction using Hansen solubility parameters [12]. Heterogeneous growth (layer per layer) occurs for dodecanoic acid-coated NPs as pure hexane is a good solvent for the alkyl chains; it results in the formation of a film (Fig. 1a). The presence of ethanol, which is a bad solvent for the alkyl chains, modifies the NPs solubility and favors their aggregation. It has been computed in a previous study that the interparticle interaction becomes attractive for an ethanol content above ca. 15% [11]. It favors the germination of supercrystals seeds in solution (homogeneous growth) that will deposit onto the substrate at some stage of their growth. These growing conditions result in a better packing and a more efficient size

segregation may be also at play. The smaller interparticle gap ($D_{i\text{-}p}$) observed in these single supercrystals is probably related to a lesser solvent swelling of the organic crown.

*3.2. Annealing effect on the structural properties of fcc supercristalline films and fcc colloidal crystals of $Co_{fcc}$ NPs*

**As-synthesized cobalt NPs are polycrystalline [13]. A transition to a single-crystalline hcp structure can be induced by annealing treatment at 350 °C [14]. During the heating step, no oxidation and coalescence between NPs are detected.**

*3.2.1. The supercrystalline films*

The GISAXS of annealed supercrystalline films (inset of Fig. 1d) shows that the fcc mesostructure is maintained without any structural damage. Besides, the (111) stacking periodicity decreases by about 0.4 nm, which is attributed to a decrease in *Di-p* from 3 nm to 2.4 nm (Table 1). The HWHM of the (111) reflection decreases from 0.08 nm to 0.06 nm, indicating an increase in the coherence length of the superstructure compared to the native sample. As a consequence of the lattice shrinking, we observe the appearance of cracks in the thinner region of the film. This behavior is in very good agreement with previous study reported for similar supercrystalline film samples [14].

*3.2.2. The colloidal crystals*

After their annealing, SEM study evidences that colloidal crystals also remain highly stable. Indeed, we do not detect changes in shape compared to the native sample, nor coalescence between crystals: compare images from the same area in Fig. 1b and e. As for the film morphology, corresponding GISAXS pattern (Fig. 1f) reveals similar features compared to the native sample, showing that long-range fcc ordered superstructure is maintained. The (111) peak remains resolution-limited ($\boldsymbol{\delta}$=0.05 $nm^{-}$

[1]). Compared to the native sample, a slight decrease in the (111) stacking periodicity is observed that reflects a decrease in the nanoparticle distance $D_{i\text{-}p}$ from 2.5 nm to 2.2 nm (Table 1). The high thermal stability of colloidal crystals of $Co_{hcp}$ NPs as well as their long-range ordering are further evidenced by high-resolution SEM technique. Thanks to the evaporation of the excess of dodecanoic acid at their surface during the heating step, extensive use of this powerful technique is allowed, which is not possible with native samples. HR-SEM study evidences long-range NP stacking for both the side and top facets for both sample morphologies. This point is illustrated by the inset of Fig.1e by the top view of a truncated triangle single-crystal case. The combination of HR-SEM and GISAXS allow to conclude that colloidal crystals of $Co_{hcp}$ NPs with long-range 3D fcc ordering are formed. This result constitutes the first example of NPs with a high magnetic anisotropy regularly packed in fcc colloidal single-crystals.

The effect of annealing is almost similar for both morphologies and results in a decrease of the interparticle distance $D_{i\text{-}p}$,. This behavior can be attributed to the increased motion of the alkyl chains surrounding the NPs, during their heating at temperature above their melting temperature (44-46 °C) [15], the evaporation of the solvent molecules trapped in the organic crown may also play a role. Due to the smaller $D_{i\text{-}p}$, for the native colloidal crystals compared to the native supercrystalline films, this feature is more pronounced in the last case. $D_{i\text{-}p}$ = 2.2 nm appears as the minimum interparticle distance that can be reached with simple annealing.

*3.3. Comparative magnetic properties of supercristalline films and colloidal crystals of either $Co_{fcc}$ NPs or $Co_{hcp}$ NPs*

*3.3.1. Hysteresis*

Fig. 2a and b shows the hysteresis curves for the supercrystalline film and the colloidal crystals, performed at 3 K respectively. In both cases, the magnetic behavior *of the native samples (solid lines)* is almost similar to that previously observed for the supercrystalline film of $Co_{fcc}$ NPs [5]. Whatever the supercrystal morphology, saturation is reached at around 4 T with the same ratio of remanent-to-

saturation magnetization ($M_r/M_s$) of 0.5 *for the native NP samples*. However, the coercive field ($H_c$) is higher for the native colloidal crystals (920 Oe) compared to the native supercristalline film (850 Oe) (Table 1). This behavior is attributed to the higher shape anisotropy in the colloidal crystals compared to the supercrystalline film, arising from the increased coherence length assembly (Table 1). This behavior is coherent with the difference in magnetic behavior at high field, observed in poorly anisotropic disordered assemblies and highly anisotropic supercrystalline films, both composed of Co NPs [16].

We observe that the annealing of colloidal crystals induces a decrease in the coercivity, $H_c$, from 920 Oe to 820 Oe (Fig. 2b (solid and dashed lines) and Table 1). Such a change is also observed but to a lesser extend when the supercrystalline films are submitted to the same annealing (Table 1).

It is important that from the magnetization at high field, we observe a significant increase in the saturation magnetization $M_s$ with the annealing process, with the same ratio ($M_s^{(ann)}/M_s^{(nat)}$) c.a. 1.67 for the two studied morphologies.

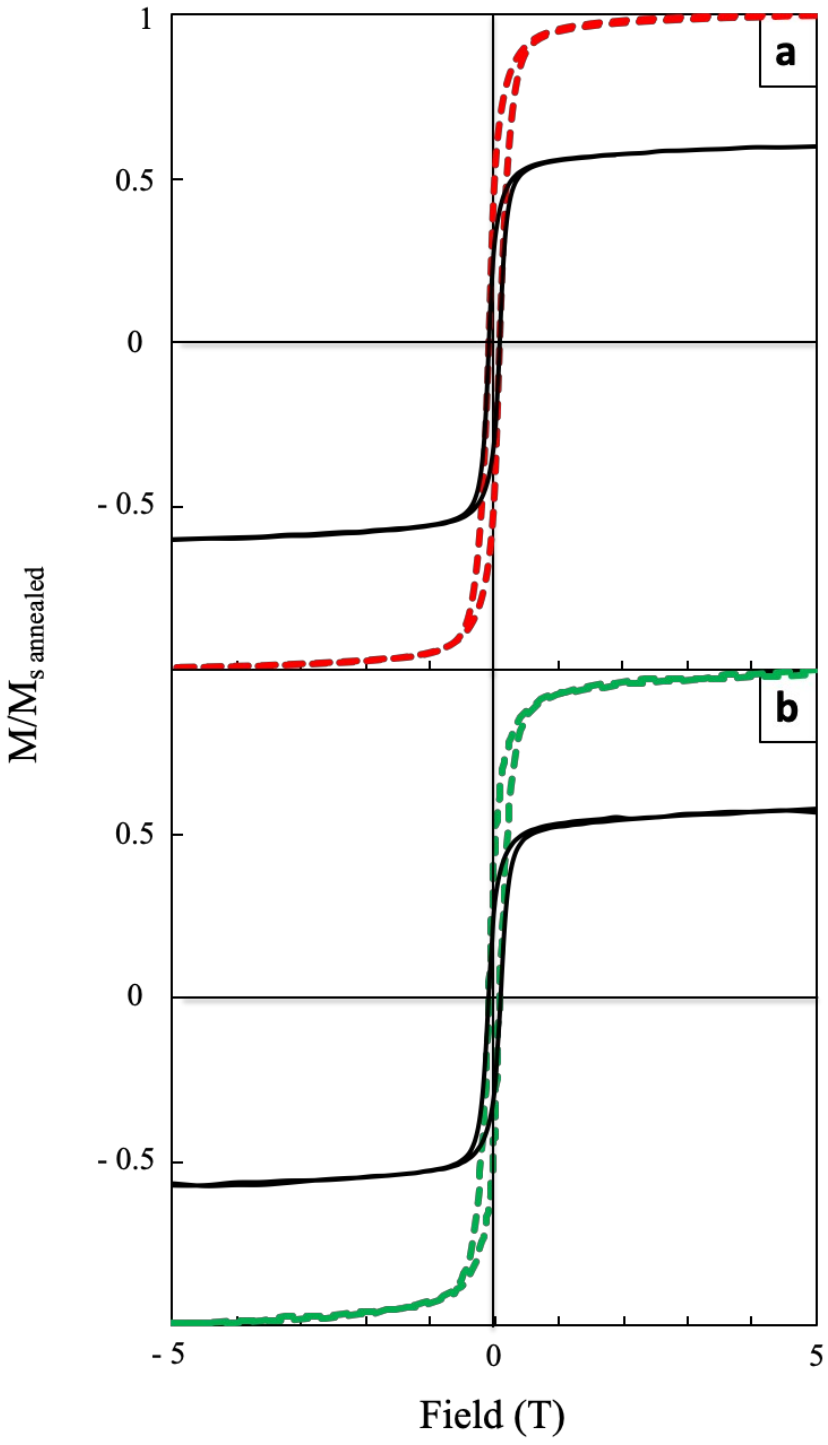


**Fig. 2.** Hysteresis curves performed at 3K of (a) supercrystalline film before (solid line) and after annealing at 350 °C (dashed line), of (b) colloidal crystals before (solid line) and after annealing at 350 °C (dashed line).

From previous works [17, 18] where $T_B$ of similar annealed Co MNP isolated and dispersed in hexane were measured, we can estimate the increase in the anisotropy constant of the NPs with the annealing process, namely ($K^{(ann)}/K^{(nat)}$) slightly larger than 3. Therefore, we conclude that the annealing induces a recrystallization of the NP leading to a change in their magnetic parameters, $M_s$ and K without modifying the morphologies of the samples. The first consequence will be an increase of the dipolar interactions through that of $M_s$ by a factor $M_s^2 \sim 2.9$ and of the magnetic anisotropy energy (MAE) through that of K by a factor ~ 3.

*3. 3. 2. ZFC/FC magnetization curves*

Fig. 3a and b shows the field cooled (FC) and zero field cooled (ZFC) magnetization curves versus temperature measured with an applied field of 20 Oe, for both supercrystalline film and colloidal crystals composed of dodecanoic acid-coated Co NPs. The native supercrystalline film (Fig. 3a, solid line) is characterized by a peak in $M_{ZFC}$ at a temperature $T_m$ of 104 K and a flat FC curve at temperature below $T_m$. This is indicative of strong dipolar interactions between the NPs as it has been evidenced in a previous study [5]. The narrowness of the ZFC peak evidences a narrow distribution of both anisotropy energies (MAE) and dipole-dipole interaction (DDI) energies related to low size polydispersity of the $Co_{fcc}$ NP (around 11%). The comparative low field magnetic study between the two native supercrystalline samples shows that the $T_m$ is significantly larger for the native colloidal crystals (Fig. 3b, solid line), reaching 128 K (Table 1). Because the two samples are made with NPs from the same synthesis batch, i.e., with the same crystallinity and size distribution, the change in $T_m$ of the ZFC peak is not induced by a change in size dispersion of $Co_{fcc}$ NPs or a difference in anisotropy. This behavior is explained by an increase in the dipolar interactions [19] arising from the decrease in the interparticle gap from around 3 nm (supercrystalline film) to 2.4 nm (colloidal crystals) (Table 1).

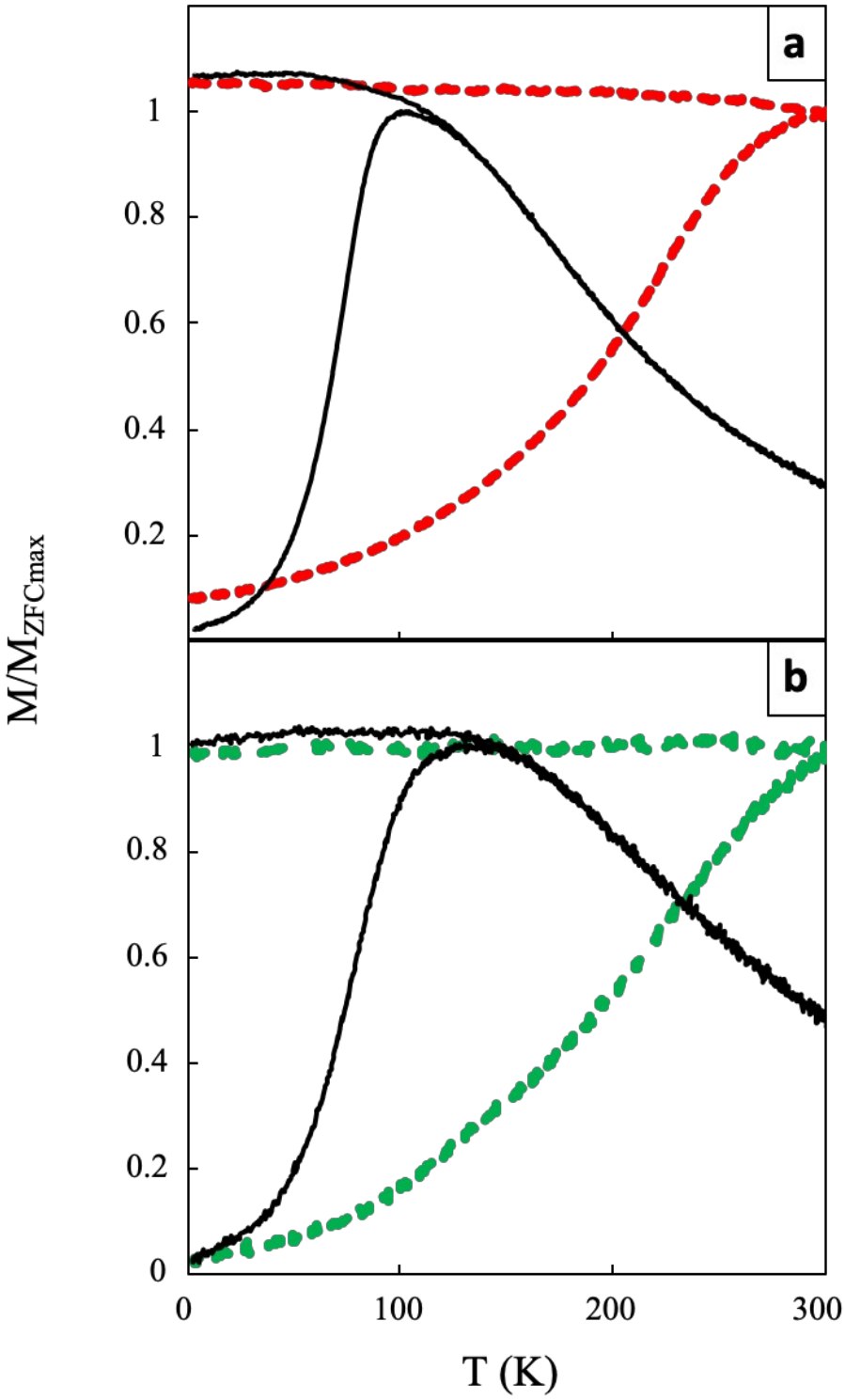


**Fig. 3.** Temperature dependence of the magnetization in the zero-field cooled/field cooled (ZFC/FC)

curves with applied field H = 20 Oe of (a) supercrystalline film before (solid line) and after annealing at 350 °C (dashed line); (b) colloidal crystals before (solid line) and after annealing at 350 °C (dashed line).

Further evidence of higher dipolar interactions in the colloidal crystals compared to the supercrystalline film is the observation of the decrease in the FC curve below $T_m$. To our knowledge, this result constitutes, the first evidence of the increase in the dipolar interactions in the colloidal crystals compared to the supercrystalline film.

In a previous publication [5], we demonstrated that the crystallographic transition of the Co NPs from a nearly amorphous fcc structure to a single-crystalline hcp structure, induced by an annealing treatment (350°C) on supercrystalline films, favors a drastic increase in the $T_m$. This highly reproducible behavior is again evidenced here and will be used as reference. Indeed, the ZFC curves for the supercrystalline films before and after annealing, reveal a drastic increase in $T_m$ from 104 K (Fig. 3a (solid line) and Table 1) to a temperature above 300 K (Fig. 3a (dashed line) and Table 1)

Focusing on the colloidal crystals, we observe that their annealing induces similar magnetic behavior. $T_m$ increases from around 128 K (Fig. 3b (solid line) and Table 1) to a temperature above 300 K Figure 3b (dashed line) and Table 1). However, from the truncated ZFC peaks (Fig. 3b dashed line) and similarly to the native supercrystals (Fig. 3a dashed line), we can observe that $T_m$ is always significantly larger for the colloidal crystals compared to the supercrystalline film. This indicates higher dipolar interactions in annealed colloidal crystals compared to the annealed supercrystalline film, which extend cannot be quantified, due to the lack of observation of a full ZFC peak. Moreover, annealing the colloidal crystals leaves qualitatively unchanged the FC curve in terms of $(T - T_m)$. Its slope remains slightly negative below $Tm$. These results highlight that, before and after their annealing, colloidal crystals always constitute stronger interacting magnetic NPs assemblies compared to the supercrystalline films.

This magnetic study shows that colloidal crystals of fcc-Co NPs, after annealing process at 350°C, transform into hard magnetic materials due to the crystallographic transformation of cobalt from fcc-Co to hcp-Co. They are harder magnetic materials compared to the annealed supercrystalline films mainly due to enhanced dipolar interactions. Moreover, this study highlights the high thermal stability against coalescence between particles and oxidation of the metal within the colloidal crystal.

The temperature $T_m$ corresponding to the maximum in $M_{ZFC}$ or the onset of $(M_{FC} - M_{ZFC}) > 0$, which coincides with the blocking temperature $T_B$ in diluted systems, is usually interpreted as the freezing temperature [20, 21] when interactions between NPs become strong enough to lead to a collective behavior of the NP moments. In Ref. [22] we determined the magnetic phase diagram of dipolar hard spheres fixed on a FCC lattice which models the colloidal crystal in the macro-spin approximation in terms of the MAE coupling measured by the ratio of the MAE ($\varepsilon_u$) to the DDI ($\varepsilon_d$) energies, $\lambda_u = \varepsilon_u/\varepsilon_d$. The result is a transition temperature, say $T_c(\varepsilon_d)$, roughly proportional to $\varepsilon_d$ in both the weak and strong coupling regimes with a proportionality factor $T_c^*(\lambda_u)$ (see Ref. [22]) which takes a value close to $T_c^*(\lambda_u=0) = 0{,}60$ and $T_c^*(\lambda_u=\infty) = 1{,}0$ in the weak and strong $\lambda_u$ coupling regimes respectively. At fixed value of the MAE, $\lambda_u \to 0$ and $\lambda_u \to \infty$ correspond to the strong and weak dipolar coupling respectively where the system undergoes either a super-ferromagnetic or a super spin-glass transition respectively in agreement with the picture outlined in Ref. [21]. When translating in terms of $\varepsilon_d$ for a fixed value of the MAE $\varepsilon_u$ this gives a transition temperature proportional to $\varepsilon_d$, with $T_f = T_c^*(\lambda_u=\infty)\varepsilon_d$ and $T_c^*(\lambda_u=0)\varepsilon_d$ in the weak and strong DDI regimes respectively. According to this picture, we expect $T_m$ to be close to the blocking temperature $T_B$ when $T_f < T_B$ , then for intermediate values of $\varepsilon_d$ when $T_m$ reaches $T_f$ a dependence of $T_m$ in between $T_c^*(\lambda_u=0)\varepsilon_d$ and $T_c^*(\lambda_u=\infty)\varepsilon_d$ and finally for very strong DDI coupling a

$T_m$ independent of the MAE and $T_m = T_c^*(\lambda_u=0)\varepsilon_d$. Preliminary Monte Carlo simulations of the FC/ZFC magnetization curves on the model used in Ref. [22] confirm qualitatively this picture.

According to this scheme, if we consider that both the colloidal crystals and the supercrystalline films present large enough DDI to be characterized by a collective behavior of their magnetic moments, as is suggested by the plateau of the $M_{FC}$ curve below $T_m$, this latter can be assimilated to the freezing temperature $T_f$ and $T_m$ should be roughly proportional to $\varepsilon_d$ , with a proportionality factor in between $T_c^*(\lambda_u=0) = 0.60$ and $T_c^*(\lambda_u=\infty) = 1.0$, and inccrease with the MAE $\varepsilon_u$ but with a weaker dependence than $\varepsilon_u$.

The estimation of the current values of both $\varepsilon_d$ and $\varepsilon_u$ is not an easy task. However, we deduced the ratio of the $M_s$ and $K_1$ values for the annealed and native samples from the magnetization measurements on the one hand and the data for the isolated Co NP on the other hand with results $(\varepsilon_d^{ann}/\varepsilon_d^{nat}) \sim 2.90$ and $(\varepsilon_u^{ann}/\varepsilon_u^{nat}) \sim 3$. Hence, unfortunately we cannot deduce from the behavior of $T_m$ upon annealing whether $T_m \sim \varepsilon_d$ or $T_m \sim \varepsilon_u$, corresponding for $T_m$ to a freezing temperature due to dipolar coupling or a blocking temperature modified by the dipolar interactions. However as already mentioned the plateau of the $M_{FC}$ curves below $T_m$ strongly suggests that we are in the former situation. Notice that upon annealing the MAE coupling constant $\lambda_u$ does not change and thus this holds also for the nature of the transition (SFM or SSG) in the hypothesis of a freezing transition at $T_m$.

## 4. Conclusions

The main purpose of this work is a focus on the annealing effect on the structural and magnetic properties of both supercrystalline films and colloidal crystals made of Co NPs. This completes our preceding work on assembly effects on supercrystalline films and colloidal crystals of polycrystalline fcc-Co NPs. One point is that from annealing process, one can change the NP magnetic properties, the

magnetic anisotropy constant and the saturation magnetization, while keeping unchanged the structure of the assemblies. The changes of $K_1$ and $M_s$ induced by annealing are deduced from preceding measurements of $T_B$ on isolated dispersion of Co NP and from the high field limit of the hysteresis loop respectively. The other point is that thanks to the fine control and optimization of the structural properties (particle anisotropy, coherence length, interparticle gap distance) of supercrystalline assemblies, we report here the first example of high-anisotropy fcc colloidal crystals composed of hard magnetic hcp-Co Nps. Although strictly speaking we cannot conclude whether the strong increase in $T_m$ upon annealing is due to that of $\varepsilon_u$ or $\varepsilon_d$, the flat plateau in $M_{FC}$ below $T_m$ seems sufficient to indicate that in the supercrystals we focus on, $T_m$ corresponds to the DDI induced freezing temperature. In this hypothesis, the increase of $T_m$ upon annealing by a factor of nearly 3 results from the increase in $\varepsilon_d$ of the same amount and is thus in agreement with the phase diagram obtained in Ref. [22].

## Acknowledgements

FEG-SEM instrumentation was facilited by the Institut des Matériaux de Paris Centre (IMPC FR2482) and was funded by Sorbonne Université, CNRS and by the C'Nano projects of the Région Ile-de-France.

**Table 1**: Structural and magnetic parameters extracted from GISAXS, the ZFC magnetization curves and the hysteresis measurements

$d_{111}$ (111): stacking periodicity, δ: width at half maximum of 111 Brag's peak, $D_{cc}$: center-to-center particle distance, $D_{ip}$: interparticle distance, $T_B$: blocking temperature, $M_r/M_s$: ratio of remanent-to-saturation magnetization, $H_c$: coercive field.

| Structural parameters | Native supercristalline films | Native colloidal crystals | Annealed supercristalline films | Annealed colloidal crystals |
|---|---|---|---|---|
| **$d_{111}$ ±0.1nm** | **9.0** | **8.7** | **8.6** | **8.4** |
| δ ± 0.01 nm | **0.08** | **0.05** | **0.06** | **0.05** |
| **$D_{cc}$ ±0.1 nm** | **11.1** | **10.6** | **10.5** | **10.3** |
| **$D_{ip}$ ±0.1 nm** | **3.0** | **2.5** | **2.4** | **2.2** |
| **$T_B$ (K)** | 104 | 128 | >300 | >300 |
| **$M_r/M_s$** | 0.5 | 0.5 | 0.48 | 0.43 |
| **$H_c$ (Oe)** | 850 | 920 | 820 | 820 |
| | | | | |
| | | | | |

**REFERENCES**


(1) M. Gauvin, N. Yang, E. Barthel, I. Arfaoui, J. Yang, P. A. Albouy, M. P. Pileni, M. P, Morphology, Nanocrystallinity, and Elastic Properties of Single Domain ε Co Supracrystals, J. Phys. Chem. C, 119 (2015) 7483–7490.

(2) J. J. Urban, D. V. Talapin, E. V. Shevchenko, C. R. Kagan, C. B. Murray, Synergism in Binary Nanocrystal Superlattices Leads to Enhanced P-Type Conductivity in Self-Assembled PbTe/Ag2Te Thin Films, Nat. Mater, 6 (2007) 115–121.

(3 ) A. Courty, I. Lisiecki, M. P. Pileni, Vibration of Self-Organized Silver Nanocrystals, J. Chem. Phys. 116 (2002) 8074–8078.

(4) I. Lisiecki, S. Turner, S. Bals, M. P. Pileni, The Remarkable and Intriguing Resistance to Oxidation of 2D Ordered hcp Co Nanocrystals. A New Intrinsic Property, Chem. Mater. 21 (2009) 2335-2338.

(5) D. Parker, I. Lisiecki, C. Salzemann, M. P. Pileni, Emergence of New Collective Properties of Cobalt Nanocrystals Ordered in Fcc Supracrystals : II , Magnetic Investigation, J. Phys. Chem. C 111 (2007) 12632–12638.

(6) I. Lisiecki, P. A. Albouy, M. P. Pileni, Face-Centered-Cubic “Supracrystals” of Cobalt Nanocrystals, Adv. Mater. 15 (2003) 712–716.

(7) M. Li, Y. Chen, N. Ji, D. Zeng, D. L. Peng, Preparation of Monodisperse Ni Nanoparticles and Their Assembly into 3D Nanoparticle Superlattices, Mater. Chem. Phys. 147 (2014) 604-610.

(8) T. Hyeon, S. S. Lee, J. Park, Y. Chung, H. Bin Na, Synthesis of Highly Crystalline and Monodisperse Maghemite Nanocrystallites without a Size-Selection Process, J. Am. Chem. Soc. 123, (2001) 12798–12801.

(9) L. Meng, W. Chen, Y. Tan, L. Zou, C. Chen, H. Zhou, Q. Peng, Y. Li, $Fe_3O_4$ Octahedral Colloidal

Crystals. Nano Res. 4 (2011) 370–375.

(10) O. Kasyutich, R. D. Desautels, B. W. Southern, J. Van Lierop, Novel Aspects of Magnetic Interactions in a Macroscopic 3D Nanoparticle-Based Crystal. Phys. Rev. Lett. 104 (2010) 1-4.

(11) A. T. Ngo, S. Costanzo, P. A. Albouy, V. Russier, S. Nakamae, J. Richardi, I. Lisiecki, Formation of Colloidal Crystals of Dodecanoic Acid Coated γ-$Fe_2O_3$ Nanocrystals Experimental and Theoretical Investigations. Colloids and Surfaces A. 560 (2019) 270-277.

(12) S. Costanzo, A. T. Ngo, V. Russier, P. A. Albouy, G. Simon, Ph Colomban, C. Salzemann, J. Richardi, I. Lisiecki, Enhanced structural and magnetic properties of fcc colloidal crystals of cobalt nanoparticles, Nanoscale. 12 (2020) 24020-24029.

(13) I. Lisiecki, M. P. Pileni, Synthesis of Well-Defined and Low Size Distribution Cobalt Nanocrystals: The Limited Influence of Reverse Micelles, Langmuir. 19 (2003) 9486-9489.

(14) I. Lisiecki, C. Salzemann, D. Parker, P. A. Albouy, M. P. Pileni, Emergence of New Collective Properties of Cobalt Nanocrystals Ordered in Fcc Supracrystals : I , Structural Investigation, J. Phys. Chem. C. 111 (2007) 12625–12631.

(15) N. Sandhyarani, M. R. Resmi, R. Unnikrishnan, K. Vidyasagar, M. Shuguang, M. P. Antony, G. Panneer Selvam, V. Visalakshi, N. Chandrakumar, K. Pandian, Y. T. Tao, T. Pradeep, Monolayer-Protected Cluster Superlattices: Structural, Spectroscopic, Calorimetric, and Conductivity Studies, Chem. Mater. 12 (2000) 104-113.

(16) I. Lisiecki, D. Parker, C. Salzemann, M. P. Pileni, Face-Centered Cubic Supra-Crystals and Disordered Three-Dimensional Assemblies of 7.5 Nm Cobalt Nanocrystals: Influence of the Mesoscopic Ordering on the Magnetic Properties, Chem. Mater. 19 (2007) 4030–4036.

(17) C. Petit, Z. L. Wang, M. P. Pileni, Seven-Nanometer Hexagonal Close Packed Cobalt Nanocrystals for High-Temperature Magnetic Applications through a Novel Annealing Process, J. Phys. Chem. B. 109 (2005) 15309-15316.

(18) Z. Yang, M. Cavalier, M. Walls, P. Bonville, I. Lisiecki, M. P. Pileni, A Phase-Solution Annealing Strategy to Control the Cobalt Nanocrystal Anisotropy: Structural and Magnetic Investigations, J. Phys. Chem. C. 116 (2012) 15723-15730.

(19) E. Tronc, P. Prene, J. P. Jolivet, F. d'Orazio, F. Lucari, D. Fiorani, M. Godinho, R. Cherkaoui, M. Nogues and J. L. Dormann, Magnetic behaviour of γ-$Fe_2O_3$ nanoparticles by mössbauer spectroscopy and magnetic measurements, Hyperfine Interact. 95 (1995) 129-148.

(20) J. A. De Toro, P. S Normile, S. S. Lee, D. Salazar, J. L. Cheong, P. Muñiz, J. M. Riveiro, M. Hillenkamp, F. Tournus, A. Tamion, P. Nordblad, Controlled Close-Packing of Ferrimagnetic Nanoparticles: An Assessment of the Role of Interparticle Superexchange Versus Dipolar Interactions, J. Phys. Chem C. 117 (2013) 10213-10219.

(21) O. Petracic, Superparamagnetic Nanoparticle Ensembles, Superlattices and Microstructures. 47 (2010) 569.

(22) V. Russier, J. J. Alonso, I. Lisiecki, A. T. Ngo, C. Salzemann, S. Nakamae, C. Raepsaet, Phase diagram of a three-dimensional dipolar model on an fcc lattice, Phys. Rev. B. 102 (2020) 174410-10